Rock and Soil Mechanics

Volume 42 | Issue 4 Article 2

8-25-2021

Effect of moisture content on characteristic stress and acoustic emission characteristics of red sandstone

Kui ZHAO
Jiangxi Provincial Key Laboratory of Mining Engineering, Jiangxi University of Science and Technology, Ganzhou, Jiangxi 341000, China

Shan-hu RAN
Jiangxi Provincial Key Laboratory of Mining Engineering, Jiangxi University of Science and Technology, Ganzhou, Jiangxi 341000, China

Peng ZENG
Jiangxi Provincial Key Laboratory of Mining Engineering, Jiangxi University of Science and Technology, Ganzhou, Jiangxi 341000, China

Dao-xue YANG
Jiangxi Provincial Key Laboratory of Mining Engineering, Jiangxi University of Science and Technology, Ganzhou, Jiangxi 341000, China, daoxuey@126.com

See next page for additional authors

Custom Citation

ZHAO Kui, RAN Shan-hu, ZENG Peng, YANG Dao-xue, TENG Tian-ye, . Effect of moisture content on characteristic stress and acoustic emission characteristics of red sandstone[J]. Rock and Soil Mechanics, 2021, 42(4): 899-908.

Effect of moisture content on characteristic stress and acoustic emission characteristics of red sandstone

Authors

Kui ZHAO, Shan-hu RAN, Peng ZENG, Dao-xue YANG, and Tian-ye TENG

Rock and Soil Mechanics 2021 42(4): 899–908 ISSN 1000–7598
https: //doi.org/10.16285/j.rsm.2020.6201 rocksoilmech.researchcommons.org/journal

Effect of moisture content on characteristic stress and acoustic emission characteristics of red sandstone

ZHAO Kui[1, 2], RAN Shan-hu[1, 2], ZENG Peng[1, 2], YANG Dao-xue[1, 2], TENG Tian-ye[3]

1. School of Resources and Environmental Engineering, Jiangxi University of Science and Technology, Ganzhou, Jiangxi 341000, China
2. Jiangxi Provincial Key Laboratory of Mining Engineering, Jiangxi University of Science and Technology, Ganzhou, Jiangxi 341000, China
3. Shenhua Nortel Shengli Energy Co., Ltd., Xilinhot, Inner Mongolia 026000, China

Abstract: In order to investigate the response law of moisture content to the characteristic stress and acoustic emission characteristics of red sandstone, the uniaxial compression tests of red sandstone under different moisture content conditions were conducted using RMT-150C rock mechanical pressure testing machine and PCI-Ⅱ AE win acoustic emission system. The physical and mechanical parameters and characteristic stress evolution mechanism of red sandstone under water erosion are analyzed, and the evolution law of acoustic emission (wide and narrow-band) time series mode under different moisture content conditions is also investigated. At the same time, the damage evolution model of red sandstone is constructed based on cumulative acoustic emission event number and statistical mechanics theory. The results show that: 1) The P-wave velocity decreases first and then increases with the increase of moisture content. When the water saturation reaches a critical value, the P-wave velocity will drop to the lowest value. 2) The acoustic emission signal received by the narrow-band receiving sensor is closely related to the friction between the particles in the red sandstone, and the acoustic emission signal received by the wide-band receiving sensor is intrinsically related to the evolution of the internal cracks in the red sandstone. 3) The moisture content has a significant effect on the acoustic emission event rate (wide-band) at the stage of unstable crack propagation, and has a minor effect on the ratio of characteristic stress to peak strength, but it has a relatively obvious effect on the strain percentage at each stage. With the increase of moisture content, the failure mode of red sandstone specimens gradually changes from brittle failure to ductile failure. 4) As the moisture content increases, a "backward" change trend can be observed for the active period of acoustic emission event rate (narrow-band), and the acoustic emission modes of dry, natural, and saturated rock samples correspond to mass shocks, pre-main-later shocks and swarm shocks type, respectively. (5) According to the damage model based on the cumulative number of acoustic emission events (wide and narrow-band), the damage process of red sandstone can be divided into four stages: initial damage stage, stable damage development stage, accelerated damage development stage and damage destruction stage.

Keywords: moisture content; characteristic stress; response frequency band; acoustic emission mode; damage coefficient

1 Introduction

Various rock engineering projects such as mining, tunnels, underground chambers, and dams are affected by groundwater or rainfall, leading to a significant reduction in the strength and deformation performance of these projects. Furthermore, various geological disasters can be induced. Therefore, investigations of rock characteristic stress and acoustic emission signal evolution under different moisture content conditions can improve the understanding of precursor characteristics of rock failure and the evolution mechanism of microcracks under hydro-mechanical coupling[1].

In recent decades, many scholars have carried out some research on the characteristic stress of rocks and made great achievements. Based on experimental results, the rock stress−strain curve is divided into five stages by Cai et al.[2], Bieniawski[3−4], Moradian[5], including stage I crack closure, stage II linear elastic deformation, stage III stable crack propagation, stage IV unstable crack propagation and stage V post-peak failure. And the stress point at the boundary of each stage is defined as the crack closure stress σ_{cc}, the crack initiation stress σ_{ci}, the crack damage stress σ_{cd}, and the peak stress σ_{ucs}, respectively. Martin[6−7] analyzed the characteristic stress of granite under load, and found that the value of σ_{ci}/σ_{ucs} ranged from 0.4 to 0.5, while the value of σ_{cd}/σ_{ucs} was about 0.8 with a small dispersion. Wang et al.[8] conducted uniaxial compression tests on red sandstone at different strain rates, and they found that σ_{ci}/σ_{ucs} of red sandstone decreased continuously with the increase of strain rate. Four methods for calculating rock characteristic stress were systematically summarized by Zhou et al.[9], including the crack volumetric strain method, the acoustic emission method, the volumetric

Received: 13 August 2020 Revised: 9 September 2020
This work was supported by the National Key Research and Development Program of China (2017YFC0804601), the National Natural Science Foundation of China (51664018) and the Outstanding Doctoral Dissertation Cultivation Program of Jiangxi University of Science and Technology (3105500025).
First author: ZHAO Kui, male, born in 1969, PhD, Professor, PhD supervisor, research interests: rock mechanics and engineering. E-mail: 296931654@qq.com
Corresponding author: YANG Dao-xue, male, born in 1990, PhD candidate, focusing on rock mechanics and engineering research. E-mail: daoxuey@126.com

strain method, and the moving point regression method. Results showed that the crack volumetric strain method was the most applicable, but it was significantly influenced by subjective factors; the acoustic emission method was the simplest to operate, but it was most affected by environmental factors. Based on the crack volumetric strain model, the pre-peak damage dilatancy and post-peak fracture dilatancy yield criteria were established, and the dilatancy and large-deformation constitutive model of the very weakly cemented rock was constructed by Meng et al. [10]. Yao et al.[11] carried out uniaxial compression tests of coal under different moisture content conditions, and they observed that σ_{ci}/σ_{ucs} and σ_{cd}/σ_{ucs} decreased with the increase of moisture content. Guo et al.[12] investigated the fracture mechanical behavior and acoustic emission characteristics of rock-like material containing 3D cracks under hydro-mechanical coupling and they found that there was a threshold for the influence of water pressure on the initiation stress and peak stress. Zhu et al.[13] demonstrated that the uniaxial compressive strength of soft coal with the different porosities increased first and then decreased with the moisture content and the critical moisture content corresponding to the peak strength had a certain difference.

The nature of the rock deformation and failure process is the evolution process of closure, initiation, propagation, and nucleation of microcracks. In this process, the strain energy inside the rock will be quickly released in the form of elastic waves, resulting in acoustic emission (AE) [14−15]. Therefore, there is a relationship between the damage evolution mechanism of microcracks inside the rock and the AE signal[16−17], which has laid the foundation for the application of AE technology in the field of rock mechanics and engineering. In recent decades, AE technology has been widely used in rock mechanics and engineering as a non-destructive monitoring technology and has made great achievements. Deng et al.[18] studied the fracture mechanical properties and AE characteristics of granite under different moisture content conditions, and found that the fracture toughness of granite gradually decreased with the increase of moisture content. Additionally, significant changes can be observed in AE characteristics of granite. Moreover, Li et al.[19] found that the concentration degree and intensity of AE energy gradually decreased with the increase of moisture content. Mogi[20] investigated AE characteristics of different materials and found that there were three basic types of AE mode, including mass shock, pre-main-later shock and swarm shock. The damage evolution functions were established by Zhang et al.[21] based on the Weibull probabilistic density function and it was found that there were also three fundamental types of AE mode including mass shock, pre-main-later shock and swarm shock as the homogeneity varies from low to high. Liu et al.[22] proposed a method for developing a damage evolution model of coal under uniaxial compression based on the normalized cumulative AE ringing count and investigated the damage characteristics during the deformation and failure process of the coal. The rock damage evolution model was also established based on the AE ringing counts under triaxial compression by Yang et al.[23] and Sun et al.[24], and they divided the damage evolution process of rock into the following four stages: initial damage stage, stable damage development stage, accelerated damage development stage and damage destruction stage.

Based on the above literature analysis, we can conclude that a lot of research has been done for investigating the evolution of rock characteristic stress and AE characteristics under different moisture content conditions. However, most of the research focuses on use of single type of AE receiving sensor to collect and analyze the AE information in the process of rock deformation and failure. There are still limited literatures investigating the relationship between the evolution mechanism of microcracks in the rock under different moisture content conditions and the AE signals collected by AE receiving sensors with different types of response frequency bands. In this study, uniaxial compression and AE tests on red sandstone are conducted under different moisture content conditions, and the relationship between the different characteristic stress stages of the red sandstone and the AE event rate (wide-band) are discussed. The evolution characteristics of AE (narrow-band) modes under different moisture content conditions are also revealed. Moreover, the evolution characteristics of damage coefficients during the deformation and failure of red sandstone are studied based on Weibull distribution and the cumulative number of AE events (wide- and narrow-band). The research results of this study can provide a theoretical basis for the design optimization and stability evaluation of rock engineering under water erosion.

2 Specimen preparation and test device

2.1 Specimen preparation

The red sandstone from southern Jiangxi province in China is sampled as the research object. To reduce the discreteness of the test data, the rock specimen materials used in the test are all taken from the same rock block. Based on the test procedures of the International Society for Rock Mechanics and Rock Engineering (ISRM), standard cylindrical rock specimens with a diameter of 50 mm and a height of 100 mm are prepared, and there are no visible defects (joints, pores

and cracks) on the surface of the rock specimens. In addition, the parallelism for the end face of the red sandstone specimen is controlled within ±0.02 mm, and the end face and the axis of the rock specimen are ensured to be perpendicular to each other to reduce the end effect during the test. The natural saturation method is used to make the red sandstone specimens in the saturated state. The specific operating steps are summarized as follows. First, the processed rock specimens are divided into three groups: G, Z, and B. The rock specimens in groups G and B are desiccated. When these specimens are cooled to ambient temperature, their P-wave velocities are measured, respectively. The rock specimens in group G are waxed, sealed, and stored in closed glass containers. The rock specimens in group B are saturated with water: these specimens are put into a water tank, and water is added to 1/3 of the height of the specimens. Two hours later, water is added to 2/3 of the height of the specimens. Four hours later, the rock specimens are submerged in water and soaked for 120 h to assure that they are fully saturated with water. The P-wave velocities are also measured for these saturated rock specimens. After these steps, the rock specimens in group B are waxed, sealed, and stored in closed glass containers. Additionally, the P-wave velocities of specimens in group Z are measured; and the specimens are waxed, sealed, and stored in closed glass containers. Based on the average dry mass of the dry and saturated rock specimens, it is estimated that the average natural moisture content of the selected rock specimens is about 1.46%.

2.2 Test device

The loading test is carried out using RMT-150C rock mechanics testing system with the loading mode of axial displacement control and the loading rate of 0.002 mm/s. The PCI-II AE win type acoustic emission hardware system developed and produced by American Physical Acoustics Company complete with its supporting software system is adopted, which can collect and process AE parameters and waveform data in real time. In order to investigate the AE response characteristics of different frequency bands during the deformation and failure of red sandstone under different water content conditions, two AE probes with different response frequency ranges (R15α and Nano30) are used in this test, and their response frequency ranges are 50−200 kHz and 125−750 kHz, respectively. To simplify the analysis process, the AE signal collected by R15α is defined as the AE signal of the narrow-band receiving sensor and the AE signal collected by the Nano30 is defined as the AE signal of the wide-band receiving sensor. Moreover, the pre-gain of the two receiving sensor amplifiers is set to 35 dB with a threshold of 40 dB. The sampling frequency is 1MHz, and the AE signal length is set to 1 024. To make sure of sufficient coupling between the AE probe and the specimen, a layer of vaseline is evenly applied on the contact surface between the AE probe and the rock specimen.

3 Analysis of test results

3.1 Test results

To investigate the characteristics of the physical and mechanical parameters of red sandstone specimens with different moisture contents under uniaxial compression, the statistical analysis is made for the relevant data from the test as listed in Table 1. With the increase of moisture content, an exponential decline is witnessed for the uniaxial compressive strength and elastic modulus of red sandstone specimens, which is basically consistent with the previous test results[25]. The average uniaxial compressive strength and elastic modulus of the red sandstone specimens in the dry state are 97.80 MPa and 9.77 GPa respectively; the average uniaxial compressive strength and elastic modulus of the red sandstone specimens in the natural state are 70.68 MPa and 8.46 GPa, respectively; and the average uniaxial compressive strength and elastic modulus of the red sandstone specimens in the saturated state are 56.22 MPa and 6.25 GPa, respectively.

Table 1 Test data of basic mechanical parameters of red sandstone specimens

Specimen No.	Hydrated state	Average moisture content /%	Uniaxial compressive strength /MPa	Average compressive strength /MPa	Elastic modulus /GPa	Average elastic modulus /GPa	Wave velocity /(m • s^{-1})	Average wave velocity /(m • s^{-1})
H-G1			99.04		9.63		2 649	
H-G2	Dry	0.00	99.39	97.80	10.50	9.77	2 638	2 646
H-G3			94.96		9.19		2 650	
H-Z1			72.45		8.87		2 463	
H-Z2	Natural	1.46	72.32	70.68	8.29	8.46	2 446	2 455
H-Z3			67.27		8.23		2 455	
H-B1			53.00		5.94		2 727	
H-B2	Saturated	2.76	55.83	56.22	6.16	6.25	2 741	2 726
H-B3			59.84		6.66		2 711	

The P-wave velocity of red sandstone specimens first decreases and then increases as the moisture content increases. When the water saturation of the rock reaches a critical value, the P-wave velocity drops to the minimum value[26−27]. This is because the wave velocity dispersion and energy attenuation happen when the elastic wave propagates in an imperfectly elastic medium. The homogeneity, porosity, particle regularity of the imperfectly elastic medium and the contact interface of different media are the most important factors affecting the dispersion of the ultrasonic velocity[28]. With the increase of moisture content, an increase followed by a decrease in the number of contact interfaces between free water and air is observed in the pores of red sandstone specimens (see Fig.1). As a result, the P-wave velocity of red sandstone specimens first decreases and then increases as the moisture content increases. However, the changing trend of the P-wave velocity is asymmetric V-shaped due to the fact that the velocity dispersion of ultrasonic propagation in water is more serious than that of propagation in the air. Therefore, we can conclude that the propagation rate of elastic wave in red sandstone is dominated by many factors including pore distribution, filling degree, and filling medium type.

3.2 Characteristic stress

According to the axial stress−strain characteristics of the rock specimen under uniaxial compression, the rock stress−strain curve is divided into five stages by Bieniawski[3] and Moradian et al.[5], including stage I crack closure, stage II linear elastic deformation, stage III stable crack propagation, stage IV unstable crack propagation and stage V post-peak failure. At present, some methods including the AE method, the crack volumetric strain method, the moving point regression method, and the lateral strain method are used to classify rock characteristic stress stages by many researchers. Martin[7] first proposed the concept of crack volumetric strain method and used it to study the characteristic stress of granite in the early 1990s. This method can improve the accuracy of determination of the closure stress and initiation stress of rock cracks to a certain extent. It is widely used for investigation of rock characteristic stress because it has a clear physical meaning and the calculation is relatively simple and convenient. The schematic of the crack volumetric strain method is displayed in Fig.2. The rock volumetric strain and crack volumetric strain under uniaxial compression are calculated as follows[9]:

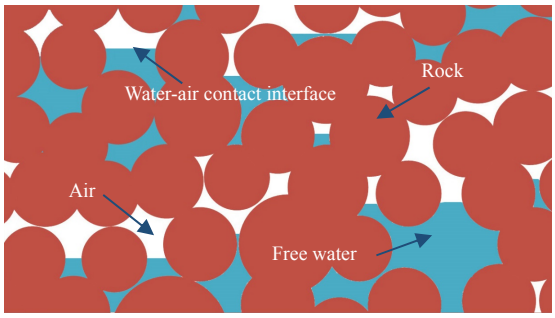

Fig. 1 Schematic of water filling in some pores of red sandstone

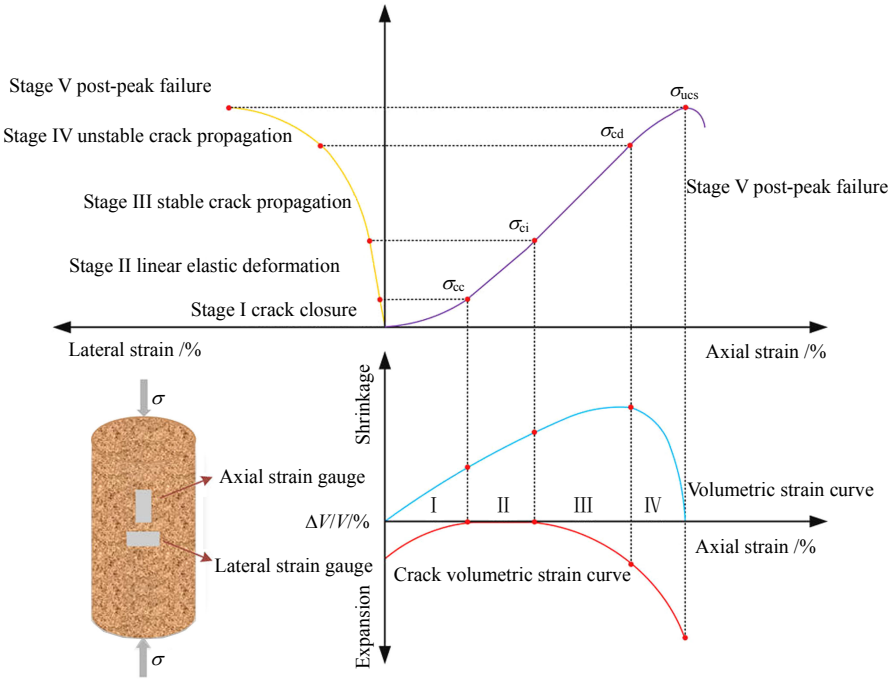

Fig. 2 Schematic of stress stage division and characteristic stress determination

The rock volumetric strain is

$$\varepsilon_{\mathrm{v}}=\frac{\Delta V}{V}\approx\varepsilon_1+2\varepsilon_2 \tag{1}$$

where ε_{v}, ε_1 and ε_2 correspond to volumetric strain, axial strain, and radial strain, respectively. The total strain of the rock material can be approximately equal to the sum of the elastic volumetric strain $\varepsilon_{\mathrm{v}}^{\mathrm{e}}$ and the crack volumetric strain $\varepsilon_{\mathrm{v}}^{\mathrm{c}}$. Therefore, the crack volumetric strain can be calculated by

$$\varepsilon_{\mathrm{v}}^{\mathrm{c}}=\varepsilon_{\mathrm{v}}-\varepsilon_{\mathrm{v}}^{\mathrm{e}}=\varepsilon_{\mathrm{v}}-\frac{1-2\mu}{E}\sigma \tag{2}$$

where $\varepsilon_{\mathrm{v}}^{\mathrm{e}}$, $\varepsilon_{\mathrm{v}}^{\mathrm{c}}$, μ and σ represent the elastic volumetric strain, the crack volumetric strain, Poisson's ratio and the axial stress, respectively.

The volumetric strain and crack volumetric strain curves of red sandstone specimens with different moisture contents can be calculated based on Eqs. (1) and (2). Due to space limitations, the specimen H-G1 in the dry state, the specimen H-Z1 in the natural state, and the specimen H-B1 in the saturated state are taken as examples (see Fig.3) in this study to investigate the relationship between the characteristic stress of red sandstone specimens and the AE event rate (wide-band) under different moisture content conditions.

According to Fig.3, the characteristic stress, volumetric strain, crack volumetric strain, and AE event rate (wide-band) curves of red sandstone specimens with varying moisture contents have certain similarities at stages I, II, and III, but have a certain difference at the stages IV and V.

The ratio of characteristic stress to peak stress of red sandstone specimens at different moisture contents (see Table 2), and the coupling relationship between the AE event rate (wide-band) and the characteristic stress stage are as follows:

(1) Stage I crack closure. At this stage, a concave upward trend can be observed in the stress−strain curve. The original microcracks and pores in the rock are continuously compacted, and the crack volumetric strain gradually approaches a stable value. This stage ends when σ_{cc} of the rock is achieved, and the moisture content ratio (see Table 2) almost has no effect on $\sigma_{\mathrm{cc}}/\sigma_{\mathrm{ucs}}$. Additionally, the number of AE events (wide-band) generated by the red sandstone specimens in the dry and natural states is larger than that generated in the saturated state. This is because of the gradual closure of the original microcracks and pores in the rock specimen under the lower load. A small number of rough and weakly cemented surfaces are broken during the closing process, and then a part of the AE signal with relatively low energy is generated. The energy attenuation rate of the AE signal in the propagation process in the water medium is much greater than that in the rock skeleton and the air. As a result, some of the AE signal amplitudes are lower than the preset AE threshold, which can be regarded as noise signals and filtered out. Therefore, a gradual decrease can be detected in the number of AE events (wide-band) at the crack closure stage as the moisture content increases.

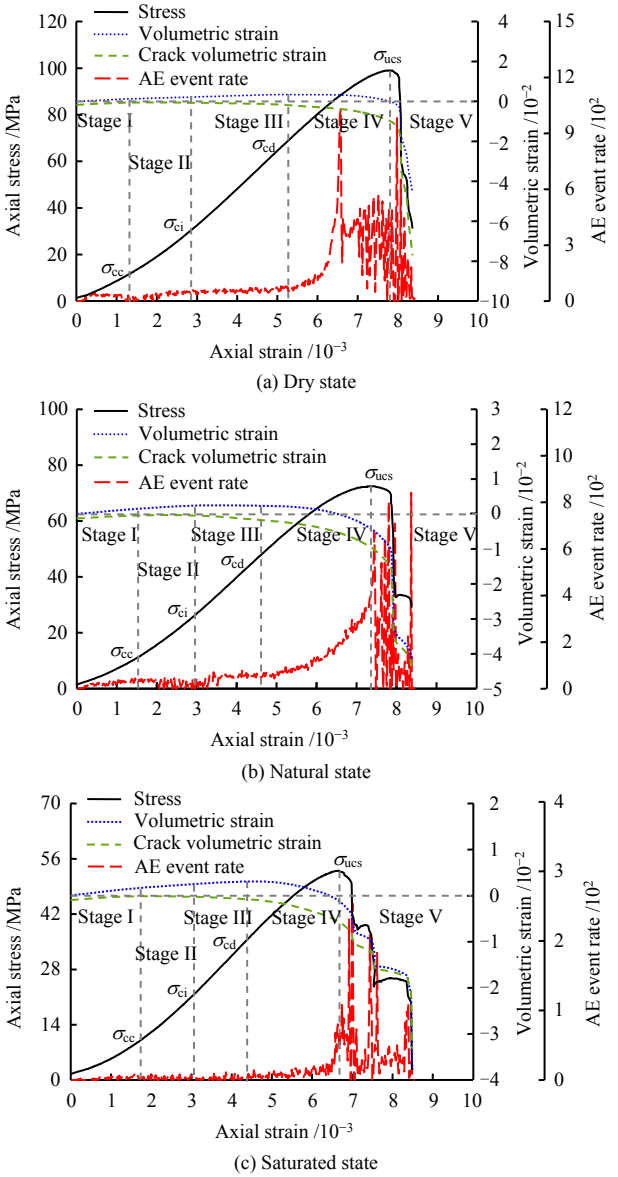

Fig. 3 Relationship between characteristic stress stage and acoustic emission event rate (wide band)

Table 2 Normalization table of characteristic stress

Specimen No.	Hydrated state	$(\sigma_{\mathrm{cc}}/\sigma_{\mathrm{ucs}})$ /%	Average	$(\sigma_{\mathrm{ci}}/\sigma_{\mathrm{ucs}})$ /%	Average	$(\sigma_{\mathrm{cd}}/\sigma_{\mathrm{ucs}})$ /%	Average
H-G1		20.56		42.23		68.29	
H-G2	Dry	20.63	20.64	41.09	41.33	67.90	67.84
H-G3		20.74		40.68		67.34	
H-Z1		20.01		40.28		70.53	
H-Z2	Natural	19.15	19.50	39.39	39.58	69.57	68.28
H-Z3		19.33		39.07		64.75	
H-B1		18.98		37.79		59.98	
H-B2	Saturated	19.83	18.71	37.42	37.74	58.14	59.82
H-B3		17.33		38.02		61.35	

(2) Stage II linear elastic deformation. At this stage, a linear trend can be observed in the stress−strain curve. The original microcracks and pores in the rock are compacted with no further development. The crack volumetric strain remains relatively stable, and the AE (wide-band) activity is also relatively stable. The stress at this stage is not large enough to cause secondary microcracks in the rock, and this stage ends when σ_{ci} of the rock is achieved. Moreover, the moisture content has a minor effect on σ_{ci}/σ_{ucs} of red sandstone specimens.

(3) Stage III stable crack propagation. A convex upward trend is observed in the stress−strain curve at this stage. The original cracks inside the rock begin to propagate, and the secondary cracks start to initiate and propagate at the same time. This stage ends when σ_{cd} of the rock is achieved and the crack volumetric strain starts to increase slowly during this stage. The number of AE events (wide-band) generated by the red sandstone specimens in the dry and natural state increases slowly as the test time increases. The change of the AE event rate (wide-band) generated by the specimens in the saturated state is similar to that at the linear elastic deformation stage, with a relatively stable development trend. The values of σ_{cd}/σ_{ucs} of the red sandstone specimens in the dry and natural state are 10% larger than that in the saturated state. This phenomenon is because the pore water pressure in the microcracks and the Stefan effect have a hindering effect on the further propagation of microcracks[29−30].

(4) Stage IV unstable crack propagation. The original microcracks begin to interact with each other, and the secondary cracks develop rapidly and start to propagate and coalesce owing to loading. Under the interaction of original and secondary cracks, the microcracks in the red sandstone gradually form macroscopic cracks, which eventually leads to continuous plastic failure of the red sandstone specimens. This stage ends when σ_{ucs} of the rock is achieved and the development rate of the crack volumetric strain is higher than that at other stages. The dry red sandstone specimens produce a large number of AE events (wide-band) at this stage, and a trend of increasing-decreasing-relatively stable development can be witnessed for the rate of AE events (wide-band). However, the AE event rate (wide-band) of the red sandstone specimens in the natural state at this stage presents the trend of accelerating increase. Moreover, a slow increase followed by a rapid increase before the peak failure can be found for the AE event rate (wide-band) of the saturated red sandstone specimens. Based on the above test results, the moisture content has a significant effect on the distribution characteristics of the AE event rate (wide-band) during the unstable crack propagation stage.

(5) Stage V post-peak failure. The red sandstone specimens under the load gradually fracture along the macroscopic cracks, and the AE event (wide-band) is the most active at this stage. The red sandstone specimen in the dry state loses its bearing capacity soon after reaching σ_{ucs}, and a brittle failure mode can be observed. Additionally, several drops in stress can be witnessed for the red sandstone specimens in the saturated state at the post-peak failure stage and a ductile failure mode is displayed. The results above indicate that the failure mode of red sandstone specimens gradually changes from brittle to ductile failure with the increase of moisture content.

To further investigate the influence of moisture content on the strain at each stage, a statistical analysis of the ratio of strain to total strain of red sandstone specimens with different moisture contents is conducted in this paper (see Fig.4). According to Fig.4, the strain percentage of each stage gradually decreases with the increase of moisture content within the stages from I to IV. However, the change characteristics of strain percentage are significantly different from that at the pre-peak stages: as the moisture content increases, the strain percentage at the post-peak failure stage gradually increases. According to the results above, the moisture content has a minor effect on the ratio of characteristic stress to peak strength, but it has a relatively significant effect on the strain percentage at each stage.

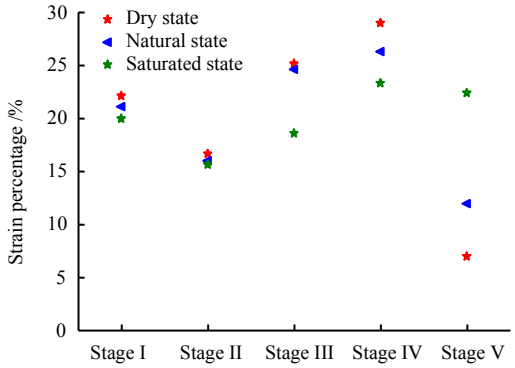

Fig. 4 Percentage of stage strain

4 AE mode and damage evolution

4.1 AE mode (narrow-band)

In order to investigate of moisture content on the AE (narrow-band) mode, the time series of AE event rates (narrow band) of red sandstone specimens under different moisture content conditions are statistically analyzed, as shown in Fig.5.

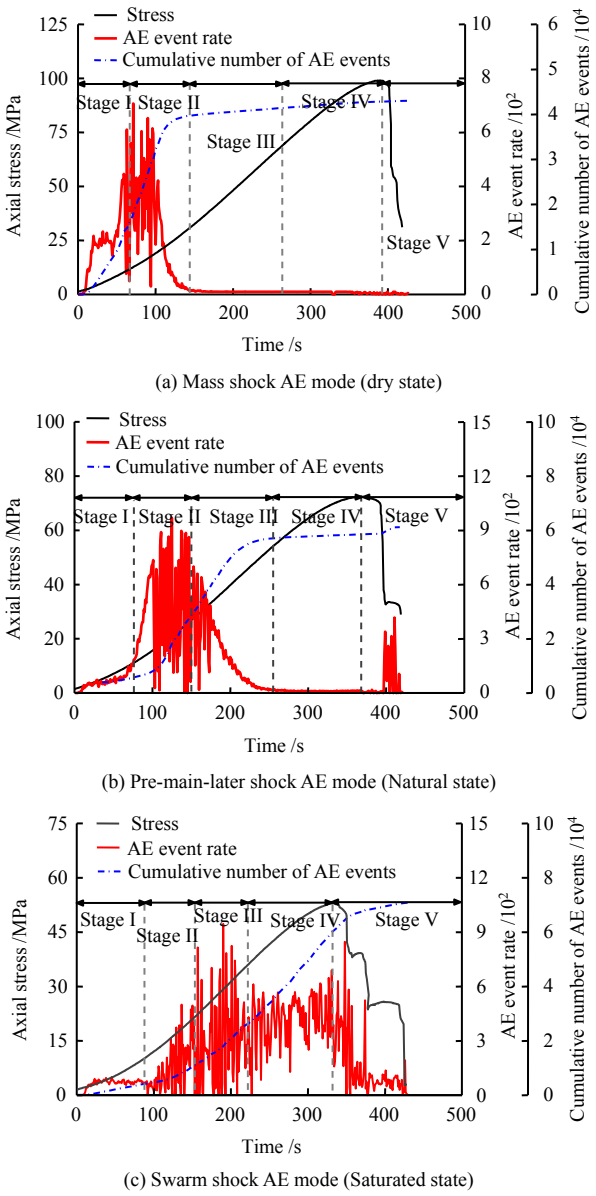

(a) Mass shock AE mode (dry state)

(b) Pre-main-later shock AE mode (Natural state)

(c) Swarm shock AE mode (Saturated state)

Fig. 5 Time series of three acoustic emission modes under different moisture contents

A "backward" change trend can be observed for the active period of AE event rate (narrow-band) as the moisture content increases as shown in Fig.5, and the AE event rate (narrow-band) of the dry red sandstone specimens is of mass shock mode. At the stages I and II, the original microcracks, pores and weakly cemented surfaces inside the rock are continuously compacted and the microcracks are gradually closed, resulting in relative slippage of microcracks and weakly cemented surfaces under the load. Then a large number of AE events (narrow-band) are produced due to friction between particles. The AE event rate (narrow-band) of the red sandstone specimens in the natural state is of pre-main-later shock mode. This is because the microstructure inside the rock is filled with free water, and the energy of the AE signal decays faster in the water. Therefore, the number of AE events (narrow-band) of the red sandstone specimens in the natural state is reduced at the stage I as compared with that of the red sandstone specimens in the dry state. Moreover, free water can reduce the friction coefficient of the interaction between the internal microstructures of the rock, and contribute to the initiation, sliding and propagation of secondary cracks at the same time, further resulting in a large number of AE events (narrow-band) at the stage III. The AE event rate (narrow-band) of the red sandstone specimens in the saturated state is of swarm shock mode. At the stage IV, the microcrack structure inside the rock is filled with free water and many secondary cracks are generated. Under the combined action of free water and load, the friction between the internal microcracks becomes more intense. So, a large number of AE events (narrow-band) are also produced at this stage. Meanwhile, a conjugate shear failure mode can be finally witnessed for red sandstone specimens in the saturated state under friction. According to the test results, the AE signal received by the narrow-band receiving sensor (response frequency 50-200 kHz) can characterize the friction between the microcrack structures in the rock. As the moisture content increases, the friction between the microcrack structures in the rock becomes more intense, and the number of produced AE events (narrow-band) gradually increases.

4.2 Analysis of damage evolution characteristics based on the cumulative number of AE events (wide-and narrow-band)

As mentioned above, the damage evolution in the process of rock deformation and failure is closely related to the AE signal. Therefore, the AE parameters can be used to characterize the damage evolution characteristics of the rock. In reference [31], a damage constitutive model is established for concrete. Based on the cumulative number of AE events (wide-and narrow-band) and statistical mechanics theory, a damage evolution model of red sandstone is proposed in this study. Additionally, an improved damage coefficient D[22−23] is used to characterize the internal damage of the rock, and to compare and analyze effects of the moisture content on the damage evolution characteristics of the red sandstone during the deformation and failure process. According to the damage evolution model and test data, the relationship between the damage coefficient D of the cumulative number of AE events (wide-and narrow-band) and the strain can be obtained as shown in Fig.6. Changes of the wide-band damage coefficient D_w and the narrow-band damage coefficient D_n are different at different stages of damage and destruction. According to Section 3.2, the wide-band AE activity is closely related to the internal microcrack evolution process of red sandstone specimens, and D_w can be used to characterize the

damage characteristics caused by the microcrack evolution during the deformation and failure of red sandstone specimens under different moisture content conditions. It can be concluded from Section 4.1 that the narrow-band AE activity is closely related to the friction between the particles in the red sandstone specimen, and D_n can be used to describe the damage characteristics caused by the friction between the particles during the deformation and failure of the red sandstone specimen under different moisture content conditions.

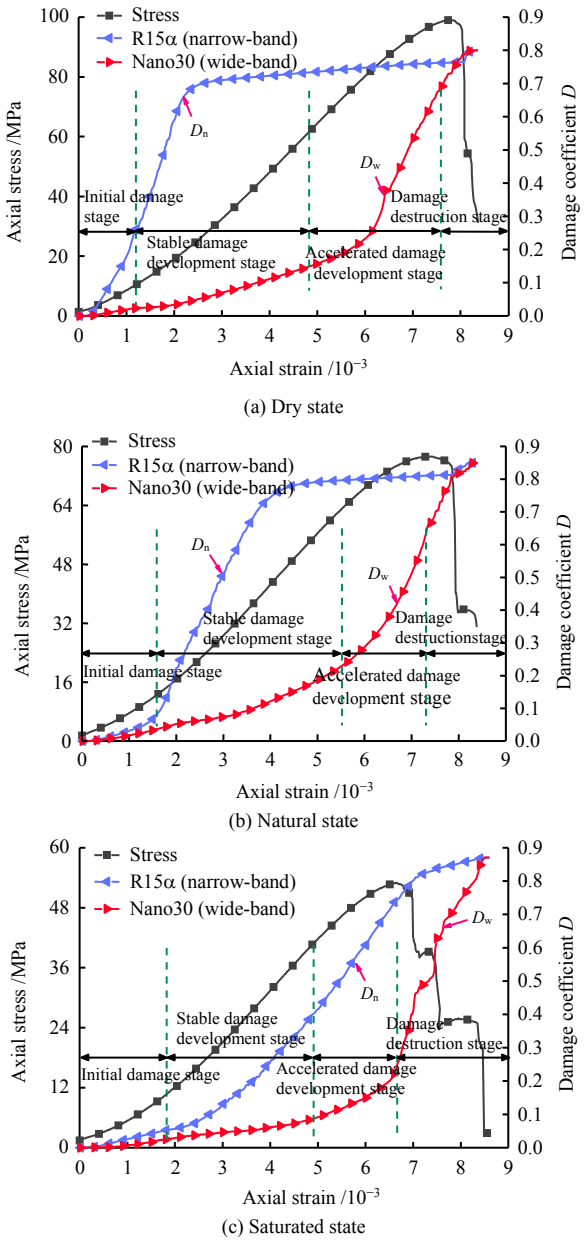

Fig. 6 Relationships between stress, damage coefficient and strain

It can be seen from Fig.6 that there are certain similarities between the growth curves of the wide- and narrow-band damage coefficients under different moisture content conditions. Therefore, the damage evolution process of the red sandstone specimens during the deformation and failure process can be divided into four stages based on the growth rate of the wide-band damage coefficient D_w.

(1) Initial damage stage. An upward trend can be found for both D_w and D_n. After the compaction of original microcracks and micropores, and particle slippage between the rough surface of the weak structure at this stage, a small number of secondary cracks can be generated. However, the growth rate of D_n is higher than that of D_w, and the growth rate of D_n gradually slows down as the moisture content increases.

(2) Stable damage development stage. The red sandstone specimen is at the stage of linear elastic deformation and the early stage of stable crack propagation. The growth rate of D_n of the red sandstone in the dry and natural state is accelerated, and the growth rate of the red sandstone specimen in the dry and natural state is greater than that of the red sandstone specimen in the saturated state. Additionally, D_w of the red sandstone specimens under different moisture content conditions approximately increases at a constant rate. At this stage, D_w gradually decreases with an increase in moisture content.

(3) Accelerated damage development stage. The red sandstone specimen is at the late stage of stable crack propagation and the stage of unstable crack propagation. The original and secondary microcracks interact with each other and the macroscopic crack can be formed in the red sandstone. At this stage, D_n of the red sandstone specimens in dry and natural state remains relatively stable, and an increasing trend cannot be observed. However, D_n of the red sandstone specimens in the saturated state increases at a constant rate. With the increase of water content, the accelerated growth rate of D_w gradually slows down.

(4) Damage destruction stage. At this stage, the red sandstone specimen slides along the macroscopic fracture surface, which accelerates the destruction of the rock specimen. Therefore, D_n that characterizes the damage caused by the internal friction of the rock increases slowly. Additionally, D_w that characterizes the damage caused by the microcrack evolution inside the rock increases continuously at an accelerating rate.

By analyzing the damage evolution process of red sandstone specimens under different moisture content conditions, the following conclusions can be drawn: under dry and natural conditions, the damage coefficient D_w obtained by the cumulative number of AE event (wide-band) is well related with the internal microstructure evolution of the rock specimen. Meanwhile, the damage coefficient D_n obtained by the cumulative number of AE event (narrow-band) under the saturated condition is closely related to the internal microstructure evolution of the rock specimen.

5 Conclusions

By investigating the characteristic stress and the evolution characteristics of AE (wide-and narrow-band) parameters during the deformation and failure of red sandstone specimens under different moisture content conditions, the following conclusions can be drawn:

(1) The P-wave velocity of red sandstone specimens first decreases and then increases as the moisture content increases, which results from the combined effect of pore distribution and filling degree of free water.

(2) The moisture content has a slight effect on the ratio of characteristic stress to peak strength, but it has a relatively significant effect on the strain percentage at each stage. With the increase of moisture content, the failure mode of red sandstone specimens gradually changes from brittle failure to ductile failure.

(3) The AE signal received by the narrow-band receiving sensor can be used to characterize the friction between the particles in the red sandstone, and the AE signal received by the wide-band receiving sensor can be used to describe the evolution of the internal cracks in the red sandstone, respectively. A "backward" change trend can be observed for the active period of AE event rate (narrow-band) as the moisture content increases. In addition, the AE modes of dry, natural, and saturated rock specimens correspond to mass shock, pre-main-later shock and swarm shock type, sequentially.

(4) The damage evolution model is established based on the cumulative number of AE events (wide-and narrow-band) and statistical mechanics theory. According to the growth rate of the wide-band damage coefficient D_{w}, the damage process of red sandstone can be divided into four stages: initial damage stage, stable damage development stage, accelerated damage development stage and damage destruction stage. Moreover, the relationships between D_{w}, D_{n} at different damage stages and moisture content are also discussed in this study.

References

[1] FANG Jie, YAO Qiang-ling, WANG Wei-nan, et al. Experimental study on damage characteristics of siltstone under water action[J]. Journal of China Coal Society, 2018, 43(Suppl. 2): 412−419.

[2] CAI M, KAISER P K, TASAKA Y, et al. Generalized crack initiation and crack damage stress thresholds of brittle rock masses near underground excavations[J]. International Journal of Rock Mechanics and Mining Sciences, 2004, 41(5): 833−847.

[3] BIENIAWSKI Z T. Mechanism of brittle fracture of rock: Part I theory of the fracture process[J]. International Journal of Rock Mechanics and Mining Sciences & Geomechanics Abstracts, 1967, 4(4): 395−406.

[4] BIENIAWSKI Z T. Mechanism of brittle rock fracture. Part II. Experimental studies[J]. International Journal of Rock Mechanics and Mining Sciences, 1967, 4(4): 407−423.

[5] MORADIAN Z, EINSTEIN H H, BALLIVY G. Detection of cracking levels in brittle rocks by parametric analysis of the acoustic emission signals[J]. Rock Mechanics and Rock Engineering, 2016, 49(3): 785−800.

[6] MARTIN C D. The strength of massive Lac du Bonnet granite around underground openings[D]. Manitoba, Canada: University of Manitoba, 1993.

[7] MARTIN C D. The progressive fracture of Lac du Bonnet granite[J]. International Journal of Rock Mechanics and Mining Sciences & Geomechanics Abstracts, 1994, 31(6): 643−659.

[8] WANG Hong-liang, FAN Peng-xian, WANG Ming-yang, et al. Influence of strain rate on progressive failure process and characteristic stresses of red sandstone[J]. Rock and Soil Mechanics, 2011, 32(5): 1340−1346.

[9] ZHOU Hui, MENG Fan-zhen, LU Jing-jing, et al. Discussion on the methods for determining the value of crack initiation strength and damage strength of hard rock[J]. Rock and Soil Mechanics, 2014, 35(4): 913−918, 925.

[10] MENG Qing-bin, WANG Jie, HAN Li-jun, et al. Physical and mechanical properties and constitutive model of very weakly cemented rock[J]. Rock and Soil Mechanics, 2020, 41(Suppl. 1): 19−29.

[11] YAO Q, CHEN T, JU M, et al. Effects of water intrusion on mechanical properties of and crack propagation in coal[J]. Rock Mechanics and Rock Engineering, 2016, 49(12): 1−11.

[12] GUO Kong-ling YANG Lei, SHENG Xiang-chao, et al. Fracture mechanical behavior and AE characteristics of rock-like material containing 3D crack under hydro-mechanical coupling[J]. Rock and Soil Mechanics, 2019, 40(11): 4380−4390.

[13] ZHU Chuan-qi, XIE Guang-xiang, WANG Lei, et al. Experimental study on the influence of moisture content and porosity on soft coal strength characteristics[J]. Journal of Mining & Safety Engineering, 2017, 34(3): 601−607.

[14] YANG Dao-xue, ZHAO Kui, ZENG Peng, et al. Numerical simulation of unknown wave velocity acoustic emission localization based on particle swarm optimization algorithm[J]. Rock and Soil Mechanics, 2019, 40(Suppl. 1): 494−502.

[15] LOCKNER D A, BYERLEE J D, KUKSENKO V, et al. Quasi-static fault growth and shear fracture energy in granite[J]. Nature, 1991, 350(7): 39−42.

[16] WU Xian-zhen, LIU Jian-wei, LIU Xiang-xin, et al. Study on the coupled relationship between AE accumulative ring-down count and damage constitutive model of rock[J]. Journal of Mining & Safety Engineering, 2015, 32(1): 28−34.

[17] LI Shu-lin, ZHOU Meng-jing, GAO Zhen-ping, et al. Experimental study on acoustic emission characteristics before the peak strength of rocks under incrementally cyclic loading-unloading methods[J]. Chinese Journal of Rock Mechanics and Engineering, 2019, 38(4): 724−735.

[18] DENG Chao-fu, LIU Jian-feng, CHEN Liang, et al. Mechanical behaviors and acoustic emission characteristics of fracture of granite under moisture conditions[J]. Chinese Journal of Geotechnical Engineering, 2017, 39(8): 1538−1544.

[19] LI Tian-bin, CHEN Zi-quan, CHEN Guo-qing, et al. An exprimental study of energy mechanism of sandstone with different moisture contents[J]. Rock and soil Mechanics, 2015, 36(Suppl. 2): 229−236.

[20] MOGI K. Earthquake prediction[M]. Tokyo: Academic Press, 1985: 20−123.

[21] ZHANG Ming, LI Zhong-kui, YANG Qiang, et al. A damage model and statistical analysis of acoustic emission for quasi-barittle materials[J]. Chinese Journal of Rock Mechanics and Engineering, 2006, 25(12): 2493−2501.

[22] LIU Bao-xian, HUANG Jing-lin, WANG Ze-yun, et al. Research on damage evolution and acoustic emission characteristics of coal and rock in uniaxial compression[J]. Chinese Journal of Rock Mechanics and Engineering, 2009, 28(Suppl. 1): 3234−3234.

[23] YANG Yong-jie, WANG De-chao, GUO Ming-fu, et al. Study of rock damage characteristics based on acoustic emission tests under triaxial compression[J]. Chinese Journal of Rock Mechanics and Engineering, 2014, 33(1): 98−104.

[24] SUN Xue, LI Er-bing, DUAN Jian-li, et al. Study on acoustic emission characteristics and damage evolution law of Beishan granite under triaxial compression[J]. Chinese Journal of Rock Mechanics and Engineering, 2018, 37(Suppl. 2): 4234−4244.

[25] ERGULER Z A, ULUSAY R. Water-induced variations in mechanical properties of clay-bearing rocks[J]. International Journal of Rock Mechanics and Mining Sciences, 2009, 46(2): 355−370.

[26] LI Min-long, LIU Hao-jie, YANG Hong-wei, et al. Experimental study on cross-frequency wave velocity and dispersion in rocks[J]. Oil Geophysical Prospecting, 2020, 55(2): 373−378, 231.

[27] CHEN Xu, YU Jin, LI Hong, et al. Experimental study of propagation characteristics of acoustic wave in rocks with different lithology and water contents[J]. Rock and Soil Mechanics, 2013, 34(9): 2527−2533.

[28] LI Wei-hua, ZHANG Zhao. Scattering of transient plane waves by deep buried cylindrical lining cavity in saturated soil[J]. Chinese Journal of Geophysics, 2013, 56(1): 325−334.

[29] ZHU Jun, DENG Jian-hui, HUANG Yi-ming, et al. Experimental study on the characteristic strength of saturated marble[J]. Chinese Journal of Rock Mechanics and Engineering, 2019, 38(6): 1129−1138.

[30] ZHENG D, LI Q B. An explanation of rate effect of concrete strength based on fracture toughness including free water viscosity[J]. Engineering Fracture Mechanics, 2004, 71(16/17): 2319−2327.

[31] GENG J S, SUN Q, ZHANG Y C, et al. Studying the dynamic damage failure of concrete based on acoustic emission[J]. Construction and Building Materials, 2017, 149: 9−16.